A study into different cell-level cooling strategies for cylindrical lithium-ion cells in automotive applications

D. Worwood[1], R.Algoo[3], R.M[c]Glen[2], J. Marco[1] and D. Greenwood [1]

[1] Warwick Manufacturing Group, University of Warwick, Coventry, UK,
[2]Thermacore Europe, Ashington, UK
[3]Jaguar Land Rover, International Digital Laboratory, Coventry, UK

Abstract: Previous research has identified that the ageing rate and performance of lithium-ion cells is negatively influenced by unfavourable cell thermal conditions, specifically, high ambient temperatures and large in-cell temperature gradients. In this paper, the effectiveness of different cell cooling strategies on reducing the in-cell temperature gradient within cylindrical cells is analysed through the development of a 2-D transient bulk layer thermal model displaying anisotropic thermal conductivity. The model is validated against experimental temperature measurements in which the peak error of the simulation was found to be 2% and 5% for the experimental test drive cycle and constant 1C discharge respectively. Results indicate that radial cooling with air or singular tab cooling with liquid may be inadequate in limiting cell temperature gradients to below 5 ℃ for HEV type 32113 cells when subject to 4 loops of the US06 drive cycle.

Keywords— Anisotropic thermal conductivity, automotive battery, thermal management, thermal modelling

1 Introduction

The worthiness of lithium-ion batteries in the automotive sector is a result of their superior energy and power density relative to previous iterations of battery technology such as lead acid and nickel-metal hydride [1]. Recent dramatic declines in cost of the lithium-ion technology [2] are also fuelling the uptake of hybrid electric vehicles (HEVs) and full electric vehicles (EV) into the automotive landscape, with forecasts predicting increased penetration rates of these vehicles within the commercial light duty vehicle market over the coming decade [3] .

Other important automotive battery metrics include life span – time the battery can satisfy the operating requirements of the vehicle, safety - which is generally associated with thermal runaway avoidance and performance – the ability of the battery to meet the vehicle operational requirements under extremes in the ambient temperature e.g. below -20 ℃ and above 40 ℃ [4]. Unfortunately these are areas where lithium-ion batteries show weaknesses, as its performance [5] and ageing rate

is highly sensitive to the operating temperature [6]. As such, in order to ensure that power and energy density are not compromised which could hamper the uptake of HEVs and EVs, the adverse temperature related effects must be mitigated through ensuring that the cell operating temperature is maintained within a range of circa $20 \pm 5℃$ [5].

Aside from the absolute value of battery operating temperature, temperature gradients present between battery cells within a pack and also between the individual cell material layers have been shown to negatively impact performance and ageing [7]–[9]. Yang et al.[9] demonstrated that temperature gradients between cells connected in a parallel string can exasperate unbalanced discharging, with the ageing rate of the battery increasing in an approximate linear fashion as the cell-to-cell temperature gradient increased. Fleckenstein et al. [8] noticed through simulation that temperature gradients present within the cell material causes inhomogeneities in cell current density, which in turn induces a local state of charge (SOC) imbalance within the cell. Specifically, an in-cell temperature gradient of 20 ℃ at the end of their duty cycle was predicted to incur a SOC gradient throughout the cell in excess of 8 %, with these inhomogeneities expected to accelerate localised ageing and in turn the overall ageing rate of the cell. Troxler et al. [7] observed experimentally that under a temperature gradient the cell performance did not perform as if the cell were operating at the volume average temperature, but rather as if at a higher average temperature than the theoretical volume average. Larger temperature gradients were observed to provide greater deviations in performance relative to the volume average operating temperature [7]. Owed to this, reports in literature suggest that temperature gradients between lithium-ion cells in a pack and through the individual cells should not exceed a maximum of 5 ℃ [9].

Attributed to these difficulties, thermal management systems are of utmost importance to ensure that these constraints on temperature are satisfied on both the cell and battery pack levels. To begin to assess whether a particular thermal management strategy is acceptable in meeting said constraints on temperature given the operating nature of the cell (e.g. duty profile), thermal modelling approaches are commonly employed as an initial stage in the design [10]. In this report a 2-D transient thermal model is developed for cylindrical cells using a finite difference approach under a homogenous bulk layer assumption for the complete cell displaying anisotropic thermal conductivity. The finite difference approach enables additional layers of fidelity to be applied to the base model during further investigation, e.g. 2-D composite material heat transfer, without the

need to develop a new model as would be required when using an analytical solution approach as in [11].

The paper is structured as follows. Section 2 outlines the development of the thermal model with Section 3 validating its accuracy against experimental temperature measurements for real 18650 cells subject to two different current profiles. The vehicle model used to obtain the electrical duty cycles used as input to the thermal model are discussed in Section 4. In Section 5 a thermal modelling study is performed on cells tailored towards EVs, plug-in hybrid vehicles (PHEVs) and HEVs when subject to their respective duty cycles. Here, the effectiveness of different cooling strategies that alter the heat transfer medium (air or liquid) and cooling location choice (radial or tab cooling) are assessed in their ability to mitigate the in-cell maximum temperature gradient (ΔT_{max}), the maximum cell temperature (T_{max}) and the volume averaged cell temperature (T_{avg}).for the given case scenarios. This enables a preliminary indication into potential acceptable cooling strategies for a given class of EV, PHEV and HEV employing cylindrical cells.

2 Thermal model

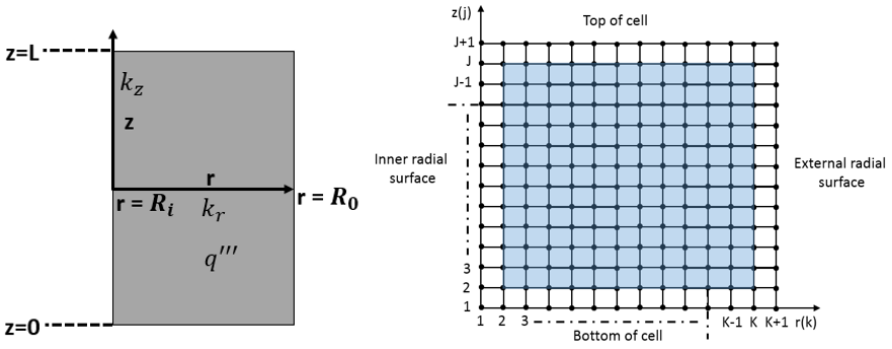

Figure 1: (left) schematic of cell geometry (right) discretised solution domain for the ADI approach

Bulk thermal models that use effective values for the cell heat capacity, density and anisotropic thermal conductivity have proven effective for thermal modelling of lithium-ion cells. An example of this approach can be viewed in [11]. Here, the complete cell (active material, electrolyte contact layer and encapsulating steel can) is treated as one homogenous material. Such models have been validated in literature against experimental cell temperature measurements and have been recommended for use in designing thermal management systems for lithium-ion cells [11]. A schematic showing the bulk layer model for the cell material is viewable in Figure 1.The governing heat conduction equation for the cell bulk material is given by:

$$\rho C_p \frac{\partial T}{\partial t} = q''' + \frac{1}{r}\frac{\partial}{\partial r}\left(k_r r \frac{\partial T}{\partial r}\right) + \frac{\partial}{\partial z}\left(k_z \frac{\partial T}{\partial z}\right) \quad (1)$$

Where ρ is the cell density [kg.m^{-3}], T the local cell temperature [K], C_p the cell heat capacity [J.kg^{-1}.K^{-1}], r and z the radial and axial positions respectively [m], R_i the radius of the cell mandrel [m], R_o the radius of the cell [m], z = 0 the location at the bottom tab of the cell [m], z=L the location at the top cell tab [m], q'' the uniform volumetric heat generation rate present within the cell [W.m^{-3}], k_r the cell effective cross-plane thermal conductivity along the r axis [W.m^{-1}.K^{-1}] and k_z the cell effective axial thermal conductivity along the z axis [W.m^{-1}.K^{-1}]. Irreversible heat generation mechanisms are considered to characterise the value of q''', whereby other heat generation terms such as entropic heating are ignored. The irreversible volumetric heat generation rate is expressed via [12]:

$$q''' = \frac{I^2 R_\eta}{v_c} \quad (2)$$

Where I is the cell current [A], R_η the overpotential resistance of the cell [Ω] and v_c the volume of the cell active material [m^3]. One common method that has proven accurate for solving the heat conduction equation in 2-D coordinates is the alternating-direction implicit (ADI) finite difference method [13], which has been adopted to solve Eq. (1). This technique discretises the heat conduction equation producing two ADI equations which are each solved in turn, given boundary conditions, using tri-diagonal matrices to determine the temperature values at the nodes within the shaded area of Figure 1 (right). Newton's law of cooling is specified at the external cell surfaces, with radiation effects neglected. An insulating boundary condition is set at r=Ri given the symmetry present within the cell. Derivation of the ADI equations is out of the scope of this paper.

3 Thermal model experimental validation

The accuracy of the thermal model is assessed against experimental temperature measurements obtained from 18650 Panasonic cells with a nominal capacity rating of 3.1 Ah subject to two test duty cycles. The cells have been placed in a climate chamber that circulates air at 25 ^{o}C. Thermocouples have been placed at the top, bottom and mid-height exterior surface of the cells facing outward from the module. Figure 2 shows the experimental set-up and an example of the

location of the thermocouples as indicated by the yellow stars. Only temperature monitored cells are shown. The 19 cells within the module are connected in parallel during testing.

Figure 2: Experimental set-up showing temperature monitored cells within a 19 cell module

The physical thermal parameters for the cell as model inputs are viewable below in Table 1.

Table 1: Test cell physical properties

k_r [W.m^{-1}.K^{-1}]	k_z [W.m^{-1}.K^{-1}]	C_p [W.m^{-1}.K^{-1}]	ρ [kg.m^{-3}]
0.25	30	1015	2418

The value for the effective cell density has been calculated given the weight of the cell (40 g) and the known volume of the cell active material (here a 3 mm cell mandrel size has been assumed based on images from [14]).

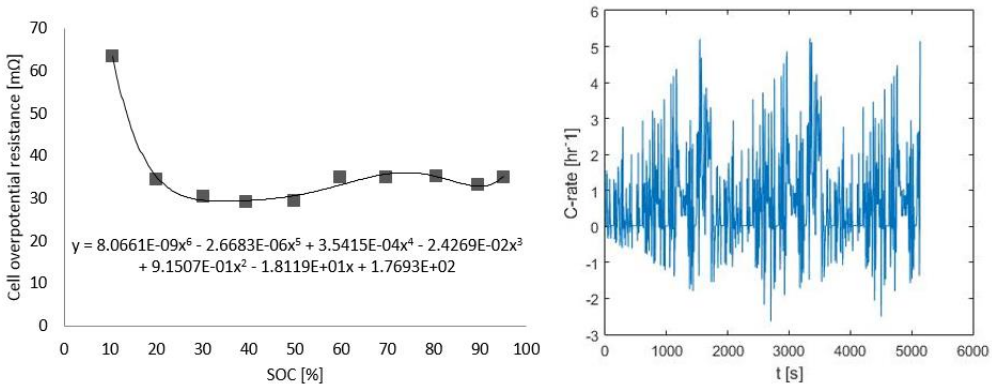

Figure 3: Experimental (left) cell overpotential resistance (right) test drive cycle c-rate profile

The value for the cell effective heat capacity is given by the cell manufacturer. The effective cross-plane thermal conductivity value has been chosen based off values that implicitly include the contribution of thermal contact resistance present between layers in the electrode assembly. These typically give rise to values in the region of 0.15-0.28 W.m^{-1}.K^{-1}, near a magnitude lower than measured values for isolated electrode assembly samples [15]. Values that include the effect of contact resistances are more representative of a complete cell structure [16] than those for isolated

electrode assembly samples or methods which calculate the effective cross-plane thermal conductivity that also ignore contact resistances. The axial thermal conductivity value is taken as that reported by Drake et al. [16].The R_η value of the cell has been measured experimentally as a function of cell SOC using the pulse method technique described in [17] using a 10 s pulse duration at 25 ^{o}C. The results can be viewed in Figure 3 (left) together with the test drive cycle cell C-rate profile (right).

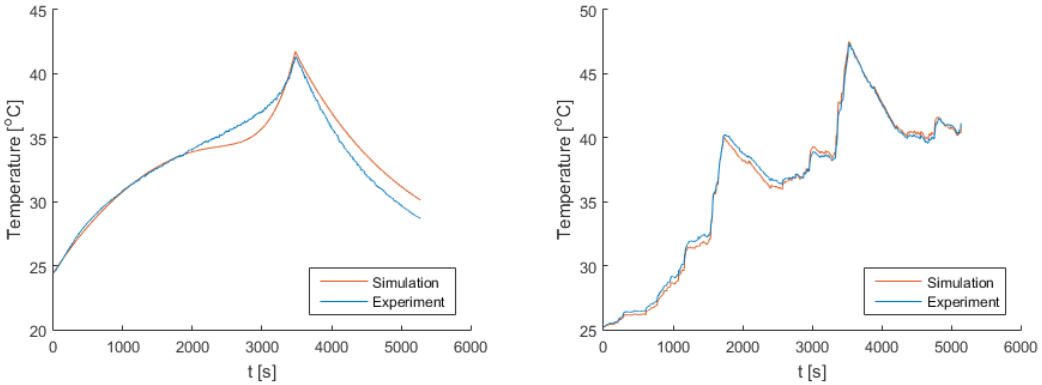

Figure 4:Mid-height outer cell surface temperature (left) constant 1C discharge (right) test drive cycle

A sub-set of the comparison results between the thermal model outputs and the experimental temperature measurement (for cell 1 as seen in Figure 2) for both test cases can be viewed in Figure 4. The convective boundary conditions employed at the radial and bottom tab surface is 6 W.m^{-1}.K^{-1}. The suggested higher value of 10 W m^{-2} K^{-1} from Shah et al. [11] is set at the top tab which is more exposed to air circulation effect from the climate chamber. Mesh resolution parameters for space and time have been chosen to ensure that the model output is independent of their value.

The model provides good agreement with the experimental measurement for both cases with a peak error of 5.3% for the 1C discharge and 2.4% for the test drive cycle duty cycles. The use of the R_η polynomial has been used for the 1C discharge, given that the deep SOC discharge results in a large increase in R_η. The model slightly under predicts the temperature within the low SOC range <17% where the large increase in R_η begins. This discrepancy may be a result of neglecting the entropic heating effect, which can be greater than 10% the value of the irreversible heat term between 0-20% SOC depending on chemistry type at 1C discharge [18]. For the test drive cycle, the cell SOC does not drop below 17% thus avoiding the region of large resistance increase and potential higher contributions from entropy heating. A nominal value of 32 mΩ has thus been used in the thermal model here to avoid Coulomb-counting given that R_η varies little between 100-17% SOC. Through

avoiding the lower SOC region, the effects of large entropy heating fluctuations are expected to be less, improving the accuracy of the assumption for sole irreversible heating. This may explain why the observed experimental error is less. Other contributions of error may arise from neglecting radiation effects, neighbouring effects from surrounding cells in the test module, the assumed values for the convection coefficient and from using a static convection coefficient value which would realistically change due to the surrounding air buoyancy effects as the cell surface temperature changes.

4 Vehicle model

A full description of the vehicle model is derived in [19] and will therefore not be repeated here. A brief overview is presented. The electrical current profiles employed were derived from a 1-D, backward-facing, lumped parameter vehicle model. The input to the EV vehicle model is the velocity profile of the US06 and WLTP drive cycle for the PHEV. Propulsion power (Pp) was derived using the standard road law equation, comprising rolling resistance and aerodynamic drag forces. The effective power at the terminals of the battery pack is reflected through the efficiency of the powertrain components (e.g. electrical machine, gearing and power electronics). During periods of regenerative braking, 24% of Pp is applied to the battery pack, with the balance dissipated as heat in the friction brakes and electric motor and inverter losses. Table 2 presents key vehicle and battery parameters considered for the model for the chosen example EV, PHEV and HEV cases. For the HEV case, the US06 power profile as presented in [20] is employed with the limit upscaled to match 40 kW, typical for the maximum power of a HEV electrical machine [21].

Table 2: Example EV, PHEV vehicle and battery parameters and HEV battery parameters

	Curb weight + 80 kg driver [kg]	Frontal area [m2]	C_d [-]	Cell type [-]	V_{cell} [V]	N_{cell} [-]	C_{cell} [Ah]	E_{pack} [Ah]
Example EV	2188	2.33	0.24	18650	3.7	7104	3.1	81
Example PHEV	1801	2.20	0.28	18650	3.7	1395	3.1	16
Example HEV	[-]	[-]	[-]	32113	3.3	96	4.4	1.4

Where C_d is the drag coefficient, V_{cell} the cell voltage [V], N_{cell} the number of cells in the battery pack, C_{cell} the nominal cell capacity [Ah] and E_{pack} the nominal pack energy [kWh].

5 Analysis

Results for the drive cycle C-rate profiles from the vehicle model for the EV and PHEV case are shown in Figure 5. The upscaled HEV cycle is also shown. For the EV and PHEV cases with 18650 cell geometry, the nominal value of 32 mΩ is used for R_η in the thermal model as deep discharges (<17 % SOC) are avoided. For the 32113 HEV cell, a nominal value of 4 mΩ is used (deep discharges also avoided) given that the cell is tailored towards high power rather than energy and designed with a higher number of current collector tabs to reduce the value of R_η. Thermal conductivity values are assumed to be the same as for the 18650 cell. This is done to remain conservative, as the measured value k_z of the isolated jelly roll sample for the 32113 cell is reported as higher at 76 $W.m^{-1}.K^{-1}$ [8] but neglects thermal resistances between the top of the jelly roll and cell terminals [8] which are implicitly include in the value for the 18650 cell as reported by Drake et al. [16]. The density of the cell is taken as 2256 $kg.m^{-3}$ given its weight of 205 g and volume (also assuming a 3 mm internal mandrel size). The effective cell heat capacity is taken as 1020 $J.kg^{-1}.K^{-1}$ as provided in [22]. Cooling boundary convective heat transfer values considered are 50 $W.m^{-2}.K^{-1}$ to reflect moderate forced convection with air [23] and 750 $W.m^{-2}.K^{-1}$ to reflect forced convection with liquid e.g. attainable with water/glycol mixture [10]. Bulk heat transfer medium and initial cell temperature are set at 25 ℃. The term radial cooling represents a positive h value at r=R_o with h=zero for other surfaces. Tab cooling represents a positive h value at the tab(s) with h=zero at the radial surface and opposite tab in the case of singular tab cooling.

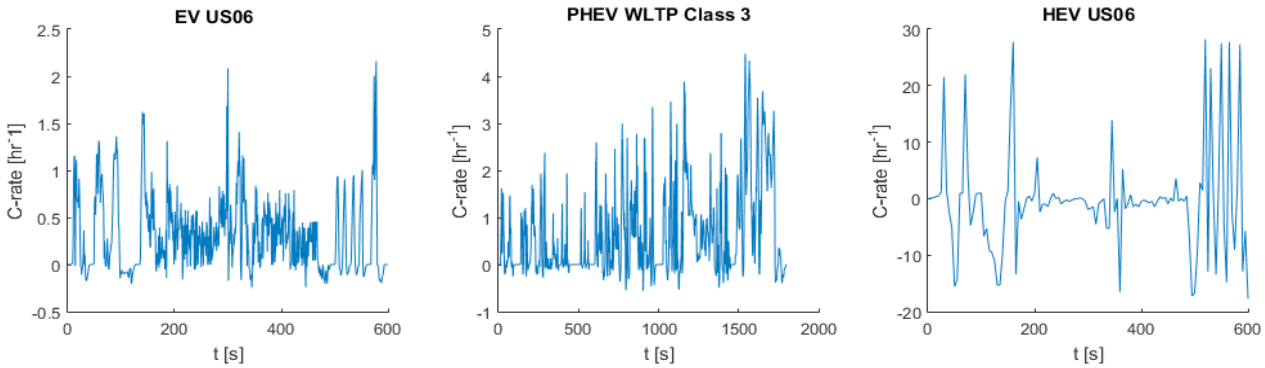

Figure 5: C-rate profile for (left) EV US06 (middle) PHEV WLTP Class 3 (right) HEV US06

5.1 PHEV model

Thermal results for the PHEV vehicle model subject to 3 loops of the WLTP Class 3 cycle are shown in Figure 6. Given the aspect ratio (diameter/length) of the cell, radial cooling with air and singular tab cooling with liquid for these h values give rise to near identical thermal results given

the overlay of the curves. Both strategies enable the peak value for ΔT_{max} to remain below 4 ℃ and T_{avg} to below 33 ℃. Double tab cooling with liquid is the most effective option as observed by the dampening effect on the thermal transients. It is, however, envisaged to be the most complex solution given that discrete tubing must be routed over both tabs for indirect liquid cooling methods.

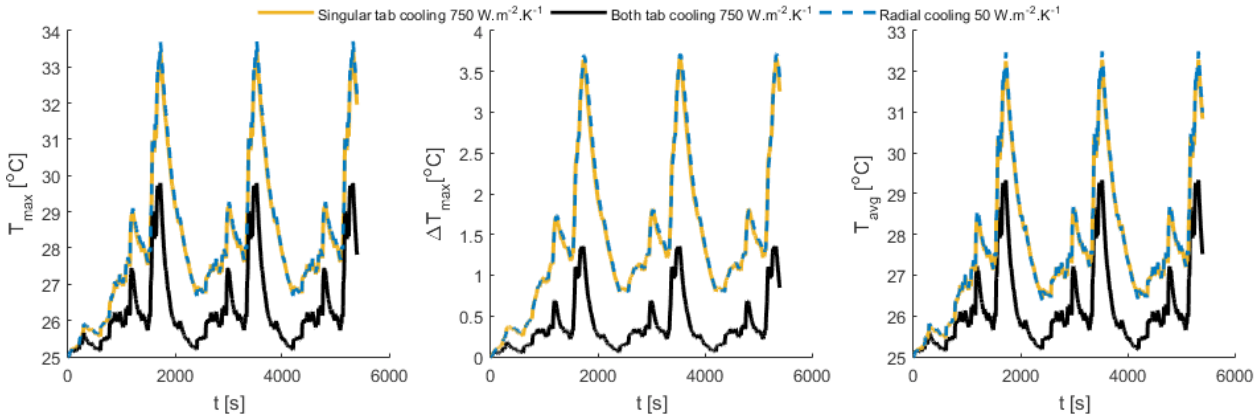

Figure 6: PHEV thermal model results for 18650 type cell subject to different cooling boundary conditions

5.2 EV model

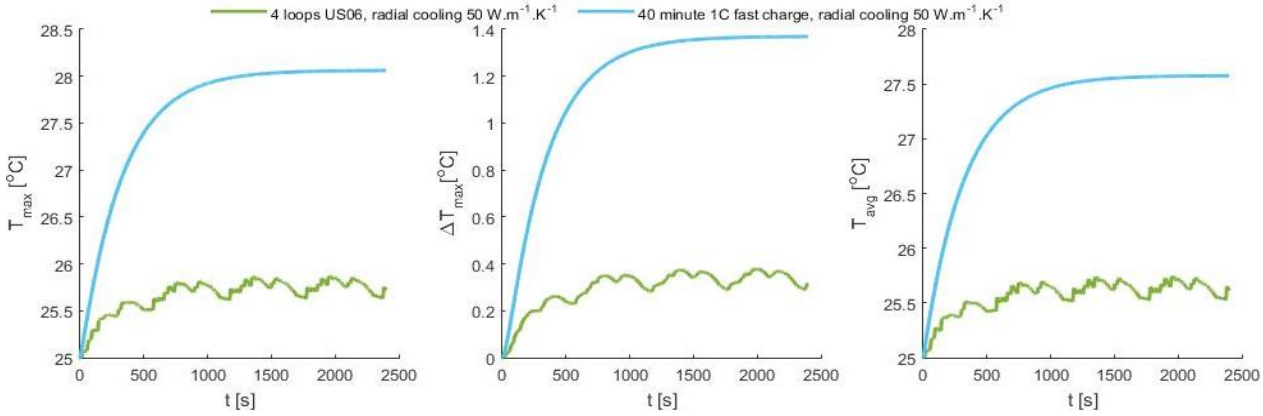

Figure 7: EV thermal model results for 18650 type cell subject to radial air cooling boundary condition

Thermal results for the EV vehicle model subject to 4 loops of the US06 cycle together with a 40 minute 1C charge (from 20% to 87 % SOC) are shown in Figure 7. Owing to the small time averaged cell heat generation rate across the US06 cycle of 0.0778 W as a result of the large pack size (81 kWh), there is a small thermal effect on the cell. The 1C charge results in a much higher time averaged heat generation value of 0.308 W resulting in a greater relative rise in T_{avg} of the cell. In both instances a basic radial air cooling approach enables ΔT_{max} to remain below 1.5 ℃.

5.3 HEV model

Thermal results for the HEV vehicle model subject to 4 loops of the US06 cycle are shown in Figure 6. For radial cooling with air and singular tab cooling with liquid, ΔT_{max} and T_{max} exceed 15 ℃ and 50 ℃ respectively during the 4th loop of the US06 HEV cycle. Introducing liquid radial cooling together with singular tab cooling offers a large reduction in both the value of T_{max} and the volume average cell temperature by more than 10℃ at t = 1970 s. However, this strategy still fails to limit the peak value of ΔT_{max} to below 15 ℃ as with the singular liquid cooled tab method. The greatest dampening effect on the value of ΔT_{max} is again observed with double tab cooling with liquid, enabling the peak value to remain below 5 ℃. Also observed through comparison with the 18650 results is that increasing the aspect ratio of the cell favours a relative improvement in the cell thermal performance of tab cooling over radial cooling for these h values. This is mainly attributed to the poor efficiency in extracting heat from the radial surface owing to the low value of k_r which is over an order of magnitude lower than k_z.

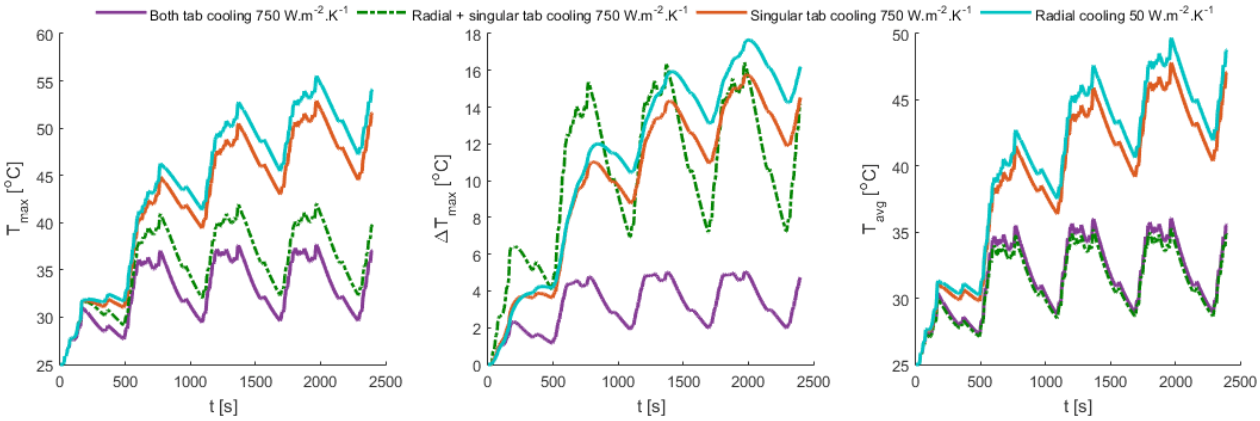

Figure 8: HEV thermal model results for 32113 type cells subject to different cooling boundary conditions

6 Conclusion

Results from the analysis indicate that air cooling across the radial surface of 18650 type high energy cells is capable of minimising the peak in cell-temperature gradient to below 4 ℃ and 2 ℃ when the cell is exercised against a duty-cycle representative of a plug-in hybrid (PHEV) and electric vehicle (EV) respectively. For high power 32113 cells subject to HEV type load-profiles, the in-cell temperature gradient can exceed 15 ℃ with singular tab or radial cooling. Double tab cooling with a liquid heat transfer medium is predicted to provide the greatest dampening effect over thermal transients within the cell at a cost of a potentially more complex cooling design.

7 Acknowledgements

The research presented within this paper is supported by the Engineering and Physical Science Research Council (EPSRC - EP/ I01585X/1) through the Engineering Doctoral Centre in High Value, Low Environmental Impact Manufacturing. The research was undertaken in collaboration with the WMG Centre High Value Manufacturing Catapult (funded by Innovate UK) in collaboration with Thermacore Europe.

8 References

[1] H. D. Yoo, E. Markevich, G. Salitra, D. Sharon, and D. Aurbach, "On the challenge of developing advanced technologies for electrochemical energy storage and conversion," *Mater. Today*, vol. 17, no. 3, pp. 110–121, 2014.

[2] B. Nykvist and M. Nilsson, "Rapidly falling costs of battery packs for electric vehicles," *Nat. Clim. Chang.*, vol. 5, no. 4, pp. 329–332, Apr. 2015.

[3] International Energy Agency (IEA), "Technology roadmap: Electric and plug-in hybrid electric vehicles," *Int. Energy Agency, Tech. Rep*, no. June, p. 52, 2011.

[4] G. Dinger, Andreas; Martin, Ripley; Mosquet, Xavier; Rabl, Maximilian; Rizoulis, Dimitrios; Russo, Massimo, Sticher, "Focus Batteries for Electric Cars," p. 18, 2010.

[5] A. Tourani, P. White, and P. Ivey, "Analysis of electric and thermal behaviour of lithium-ion cells in realistic driving cycles," *J. Power Sources*, vol. 268, pp. 301–314, 2014.

[6] T. M. Bandhauer, S. Garimella, and T. F. Fuller, "A Critical Review of Thermal Issues in Lithium-Ion Batteries," *J. Electrochem. Soc.*, vol. 158, p. R1, 2011.

[7] Y. Troxler, B. Wu, M. Marinescu, V. Yufit, Y. Patel, A. J. Marquis, N. P. Brandon, and G. J. Offer, "The effect of thermal gradients on the performance of lithium-ion batteries," *J. Power Sources*, vol. 247, pp. 1018–1025, 2014.

[8] M. Fleckenstein, O. Bohlen, M. a. Roscher, and B. Bäker, "Current density and state of charge inhomogeneities in Li-ion battery cells with LiFePO4 as cathode material due to temperature gradients," *J. Power Sources*, vol. 196, no. 10, pp. 4769–4778, 2011.

[9] N. Yang, X. Zhang, B. Shang, and G. Li, "Unbalanced discharging and aging due to temperature differences among the cells in a lithium-ion battery pack with parallel combination," *J. Power Sources*, vol. 306, pp. 733–741, 2016.

[10] G. H. Kim and A. Pesaran, "Battery Thermal Management System Design Modeling," *22nd Int. Batter. Hybrid Fuel Cell Electr. Veh. Conf. Exhib. EVS22*, vol. 1, no. November, pp. 126–133, 2006.

[11] K. Shah, S. J. Drake, D. a. Wetz, J. K. Ostanek, S. P. Miller, J. M. Heinzel, and a. Jain, "An experimentally validated transient thermal model for cylindrical Li-ion cells," *Journal of Power Sources*, vol. 271. pp. 262–268, 2014.

[12] K. Onda, T. Ohshima, M. Nakayama, K. Fukuda, and T. Araki, "Thermal behavior of small lithium-ion battery during rapid charge and discharge cycles," *J. Power Sources*, vol. 158, no. 1, pp. 535–542, 2006.

[13] M. N. Ozisik, "Finite Difference Methods in Heat Transfer." pp. 1–412, 1994.

[14] M. J. Brand, S. F. Schuster, T. Bach, E. Fleder, M. Stelz, S. Glaser, J. Muller, G. Sextl, and A. Jossen, "Effects of vibrations and shocks on lithium-ion cells," *J. Power Sources*, vol. 288, pp. 62–69, 2015.

[15] H. Maleki, "Thermal Properties of Lithium-Ion Battery and Components," *J. Electrochem. Soc.*, vol. 146, no. 3, p. 947, 1999.

[16] S. J. Drake, D. a. Wetz, J. K. Ostanek, S. P. Miller, J. M. Heinzel, and a. Jain, "Measurement of anisotropic thermophysical properties of cylindrical Li-ion cells," *J. Power Sources*, vol. 252, pp. 298–304, 2014.

[17] H.-G. Schweiger, O. Obeidi, O. Komesker, A. Raschke, M. Schiemann, C. Zehner, M. Gehnen, M. Keller, and P. Birke, "Comparison of Several Methods for Determining the Internal Resistance of Lithium Ion Cells," *Sensors*, vol. 10, no. 6, pp. 5604–5625, 2010.

[18] V. V. Viswanathan, D. Choi, D. Wang, W. Xu, S. Towne, R. E. Williford, J. G. Zhang, J. Liu, and Z. Yang, "Effect of entropy change of lithium intercalation in cathodes and anodes on Li-ion battery thermal management," *J. Power Sources*, vol. 195, no. 11, pp. 3720–3729, 2010.

[19] S. B. Peterson, J. Apt, and J. F. Whitacre, "Lithium-ion battery cell degradation resulting from realistic vehicle and vehicle-to-grid utilization," *J. Power Sources*, vol. 195, no. 8, pp. 2385–2392, 2010.

[20] V. H. Johnson, A. a Pesaran, and B. Court, "Temperature-Dependent Battery Models for High-Power Lithium-Ion Batteries," *Power*, pp. 1–15, 2000.

[21] F. Rabenstein, M. Klüting, D. F. Kessler, J. Kretschmer, C.-O. Griebel, and E. Hockgeiger, "The Full-Hybrid Powertrain of the new BMW ActiveHybrid 5," pp. 1–17, 2011.

[22] M. Fleckenstein, S. Fischer, O. Bohlen, and B. Bäker, "Thermal Impedance Spectroscopy - A method for the thermal characterization of high power battery cells," *J. Power Sources*, vol. 223, pp. 259–267, 2013.

[23] T. Bergman, A. Lavine, F. Incropera, and D. Dewitt, *Fundamentals of Heat and Mass transfer*. Chicago: John Wiley & Sons, 2011.